IEEE Access
Multidisciplinary | Rapid Review | Open Access Journal

Received April 5, 2020, accepted May 8, 2020, date of publication May 18, 2020, date of current version June 2, 2020.

Digital Object Identifier 10.1109/ACCESS.2020.2995209

Abnormal Brain Regions in Two-Group Cross-Location Dynamics Model of Autism

GENG FAN[1,2,3], YUHAO CHEN[1,2,3], YANNI CHEN[4], MING YANG[1,2,3], JUE WANG[1,2,3], CHENXI LI[1,2,3], YOUJUN LI[1,2,3], AND TIAN LIU[1,2,3]

[1]Key Laboratory of Biomedical Information Engineering, Ministry of Education, Institute of Health and Rehabilitation Science, School of Life Science and Technology, Xi'an Jiaotong University, Xi'an 710049, China
[2]Key Laboratory of Neuro-informatics & Rehabilitation Engineering, Ministry of Civil Affairs, Institute of Health and Rehabilitation Science, School of Life Science and Technology, Xi'an Jiaotong University, Xi'an 710049, China
[3]National Engineering Research Center of Health Care and Medical Devices, School of Life Science and Technology, Xi'an Jiaotong University, Xi'an 710049, China
[4]Xi'an Children's Hospital, Xi'an 710003, China

Corresponding author: Tian Liu (tianliu@xjtu.edu.cn)

This work was supported in part by the National Natural Science Foundation of China under Grant 61503295, in part by the Natural Science Foundation of Shaanxi Province under Grant 2018JM7080, in part by the China Postdoctoral Science Foundation under Grant 2018M643672, and in part by the Fundamental Research Funds for the Central Universities under Grant xjh012019049.

ABSTRACT Resting-state fMRI studies have suggested that autism spectrum disorder (ASD) is associated with aberrant dynamic changes. However, existing research either has difficulty showing the brain's dynamic characteristics or cannot obtain stable results. We examined the 'two-group cross-location hidden Markov model' of each region of interest (ROI) to identify possible pathogenic features of ASD. Specifically, we selected resting-state fMRI data with complete scales and good quality from Autism Brain Imaging Data Exchange (ABIDEI). Eligible data included 145 ASD and 157 control (CON). Two groups of subjects were separated to train Hidden Markov models representing respective populations. Then, we used each model to estimate the likelihood values of all participants. Using the likelihood value as features, we tested the significant differences of 200 ROIs and finally identified ROIs with common significant differences in the two types of models. Additionally, we investigated the relationship between likelihood values of significantly different ROIs and clinical scales. some ROIs were negatively correlated with the Autism Diagnostic Observation Schedule and positively correlated with full IQ. Finally, we constructed a support vector machine to classify ASD and CON. Overall, our findings suggested that the abnormal areas in the frontopolar area, orbitofrontal area, inferior temporal gyrus, middle temporal gyrus and fusiform gyrus are prominent features of ASD and are closely related to clinical functional decline. The average accuracy rate reached 74.9% after ten cross-validations. This 'two-group cross-localized Hidden Markov Model' provides a robust and powerful framework for understanding the dysfunctional brain architecture of ASD.

INDEX TERMS Autism spectrum disorder, resting-state fMRI, hidden Markov model, computer-assisted diagnosis.

I. INTRODUCTION

Autism spectrum disorder (ASD) is a typical derangement of brain development. ASD occurs during a momentous period of nervous system refinement that includes nerve cell proliferation, synapse formation and functional maturation of various regions. Developmental disorders lead to differences at the cerebral cortex macro anatomy level in infants and young children [1]. ASD is characterized by a collection of behavioral abnormalities such as difficulties with social interactions and verbal and nonverbal communication, repetitive behaviors, and a number of comorbid conditions [2], [3]. Although the clinical cause of autism is unclear, studies have shown structural and functional brain abnormalities. From a structural perspective, Khundrakpam et al found widespread increased cortical thickness in ASD, primarily left lateralized, with differences decreasing gradually during adulthood [3]. Diffusion tensor imaging studies show individuals with ASD have more densely packed columns of neuronal cells than normal people [4]. T1-weighted MRI has reported a

The associate editor coordinating the review of this manuscript and approving it for publication was Mohammad Zia Ur Rahman.

significantly reduced size of the posterior subregions of the corpus callosum on average and abnormal connections of the limbic-striatal region, which is the social brain system, in autistic individuals [5]–[7]. Over the years, the development of functional magnetic resonance imaging (fMRI), which measures intrinsic neural activity based on blood oxygen level-dependent (BOLD) signals, has provided a versatile tool for investigating functional mechanisms underlying cognitive dysfunction. Compared to other imaging methods, fMRI has advantages in that is non-invasive and has relatively good temporal and spatial resolution [8]. The brain does not need to perform cognitive tasks during collection of resting state fMRI (rs-fMRI) data, so this type of imaging can reflect the functional organization of the brain [9] and the hemodynamic changes caused by disease [10], [11]. The most common method of rs-fMRI data analysis uses correlation [12]–[15], partial correlation [16], [17], or sparse regression [18], [19] to build a brain functional connection (FC) network, which is a measure of synchronous activation of spatially varied brain regions [20], [21]. Based on functional connections, some autistic brain connections have been found and are different from those of healthy people. Most of the reported underconnectivity in autism is in specific brain regions or networks [22], [23], such as the default mode network, which demonstrates a consistent pattern of deactivation across a network of brain regions that includes precuneus/posterior cingulate cortex (PCC), medial prefrontal cortex (MPFC) and medial, lateral and inferior parietal cortex occurring during the initiation of task-related activity [21].

However, the method of constructing the brain network overcompresses the information on the time scale and cannot accurately reflect the internal dynamics of the brain. As shown by research, the state of the brain is a dynamic process that changes over time [24]. Many people have made attempts to find another method to describe the dynamic brain, such as calculating multiple brain connection networks based on sliding windows [25]–[27]. The limitation of sliding windows is that the size of the window is usually determined empirically. If the window is too long, it is difficult to estimate the dynamic characteristics of brain activity. If the window is too short, the number of observations is insufficient [28].

To avoid possible disadvantages in window length selection, some researchers have also begun to use dynamic Bayesian networks to generate the general framework of probabilistic models, which is often used to deal with time-varying signals with good results [29]. One of the effective methods is the Hidden Markov Model (HMM), which can describe the dynamic state switching process of the brain as a Markov chain with different transition probabilities between states [30], [31]. Due to the many excellent characteristics of HMM, it has been applied to the study of a variety of clinical diseases, among which the representative diseases include cancer [32] Alzheimer disease (AD), Huntington disease, Parkinson disease [29] and ASD [8]. Therefore, we consider the HMM to be a good model for measuring the dynamic changes in the brain time scale with good generalization ability.

In this article, we use ASD and control (CON) subjects to train the respective HMMs for each region of interest (ROI) and then use the constructed models to calculate the occurrence probability of each ROI's fMRI signal, called goodness of fit or likelihood value. Statistical analysis was used to locate areas where the dynamic state had significant differences between autistic patients and normal subjects in the two models and to discuss the clinical significance of these differential ROI. This work also used the likelihood value of the selected ROI to build a classifier. The contributions of our work can be summarized in three aspects. First, data filtering is based on multisite datasets, so the results are more scalable. Second, more representative models are trained for two groups of people, and then the intersections of areas with significant differences are chosen, so the results are more robust. Finally, the brain partitions we use are more detailed and can more accurately locate the abnormal brain areas of ASD. Our research can provide useful information for clinical studies of autism. Then, we can use the data of the characteristic regions we are looking for to construct a classifier, which is expected to achieve an accurate diagnosis of autism.

The remainder of this article is structured as follows: In the methods section, we introduce the exclusion criteria and demographic information for the data. Then, we introduce the data processing and analysis process, including data preprocessing, model construction, and classifier construction. In the results section, we summarize the abnormal brain regions exhibited by autistic patients, their relationship to clinical scales, and the performance of the classifier. The discussion section discusses the significance of the findings, the shortcomings and future perspectives.

II. MATERIALS AND METHOD

A. SUBJECTS

The present study downloaded rs-fMRI time series and acquisitions for samples of 16 international imaging sites that had aggregated and were openly sharing neuroimaging data from 539 individuals affected by ASD and 573 controls (CON), available in the ABIDE (http://fcon_1000.projects.nitrc.org/indi/abide) [7]. After a series of screenings for all datasets, 302 subjects were chosen. The selected data consisted of 145 ASDs and 157 CONs. The summary of demographics and clinical characteristics is represented in TABLE 1. Full IQ (FIQ) was measured using the Wechsler Adult Intelligence Scale, and the FIQ of CON was significantly higher than that of ASD ($p<0.01$). The Autism Diagnostic Observation Schedule (ADOS) was measured only in ASD. Data screening criteria are shown in FIGURE 1.

B. PREPROCESSING

In this research, we preprocessed datasets by the Cofigurable Pipeline for the Analysis of Connectomes (C-PAC,

TABLE 1. Summary of demographics and clinical characteristics for ASD and CON.

	ASD	CON
Age[Mean±SD]	16.39±6.52	16.07±5.72
Age range	7.13-34.46	6.47-31.78
Sex (male/%)	100%	100%
Clinical characteristics		
FIQ[Mean±SD]	107.36±16.54	112.76±12.84
ADOS[Mean±SD]	11.79±3.64	

There was no statistically significant difference in age between the two groups in the final screened data(p=0.656)

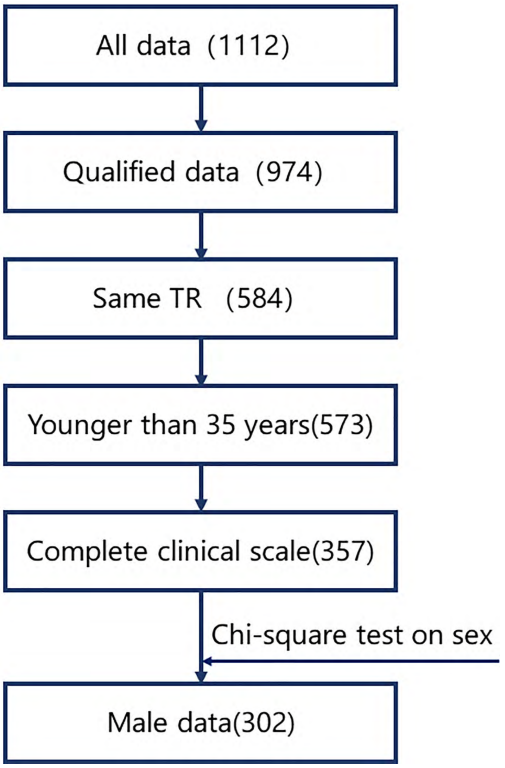

FIGURE 1. Data screening flowchart. The numbers in parentheses represent the number of participants remaining after the previous screening. 1 Exclude bad data. There are manual quality assessments of the data by three raters with columns having the prefix qc_ in the phenotypic file downloaded from the site. To obtain high quality data, we excluded the data if any rater's evaluation result was "Failed" for functional data. 2 Choose the data's repetition time as 2000 ms. The TR time was the same to ensure that the time series had the same strength standard. Data with TR equal to 2000 constituted the majority of all data. 3 Exclude the data whose age was over 35. Some research suggested that the difference in the brain between ASD and CON patients was small over the age of 35. 4 Exclude the data of subjects who lacked WASI-FIQ if the patient lacked the ADOS. For the purpose of subsequent analysis, the data from incomplete clinical scales were removed. 5 Exclude female data. A chi-square test was performed on the sex of the ASD group and the CON group, and there was a significant difference between the two groups. Female data were much less frequent than male data, so all female data were excluded.

http://fcp-indi.github.com). This python-based pipeline tool makes use of AFNI, ANTs, FSL, and custom python code. The pre-processing steps include slice time correction, motion correct to the average image, skull-strip, global mean intensity normalization to 10,000 and nuisance signal regression. Band-pass filtering (0.01-0.1Hz) was applied only for one set of strategies. Functional images were registered linearly to anatomical space and were normalized to Montreal Neurological Institute (MNI) 152 stereotactic space ($1\ mm^3$ isotropic) with linear and non-linear registrations. The regressed rs-fMRI images parcellated into 200 ROIs in the cortical regions, and then the mean across the voxels within each ROI was computed. Finally, we obtained a 200-dimensional vector sequence for each subject [33].

C. HMM

Some studies have suggested that the brain switches from one state to another. HMM is a probability model that solves the unknown hidden state by using known observation data. In this section, we will describe how to model the brain time series using an HMM framework. We will use the data of ASD and CON to construct HMMs of their populations separately (ASD MODEL and CON MODEL) and use the trained model to calculate the likelihood of all participants (FIGURE 2).

Assume the amount of data we will use to train the model is R (all ASD or CON). Every subject data has D (in fMRI data, D can be the number of voxels, regions of interest (ROI) or components). ROIs have a sequence of E-length time series. Denote the time series data as $\chi = \left\{X^{(1)}, X^{(2)}, \ldots, X^{(r)} \ldots X^{(R)}\right\}, r = 1, 2, \ldots R$, where each subject data $X^{(r)} = \left[X_1^{(r)}, X_2^{(r)}, \ldots, X_d^{(r)}, \ldots, X_D^{(r)}\right] \in R^{E\times D}$, $X_d^{(r)} = \left[X_d^{(r)}\_1, X_d^{(r)}\_2, \ldots, X_d^{(r)}\_e, \ldots, X_d^{(r)}\_E\right] \in R^E$. In this work, we support the hypothesis that (i) the temporal BOLD fluctuations of ROIs, that is to say, $X\_ROI = \left[(X_d^{(1)})^T, (X_d^{(2)})^T, \ldots, (X_d^{(r)})^T, \ldots, (X_d^{(R)})^T\right] \in R^{(E*R)}$ have their own dynamic patterns, and (ii) there may be significant differences in temporal dynamic models between ASD and CON. Based on these hypotheses, we model region-wise temporal dynamics with HMMs. It is assumed that the hidden states are changing over time with a certain probability, called state transition probability. In a transition matrix A, i.e., $A = \left[a_{ij}\right]$ each a_{ij} refers to the probability of moving from state i to state j. Moreover, each state should be initialized, i.e. $\pi = [\pi_i]$, in which each π_i refers to the probability that the initial time may be in a hidden state. In the HMM model, we mark HMMs set as $S_{ROI} = \left\{S^{(1)}, S^{(2)}, \ldots, S^{(d)} \ldots S^{(D)}\right\}$, where $S^{(d)}$ is the HMM of dth ROI and comes from a discrete state set with size K. For the dth ROI, the hidden state is denoted as $S^{(d)} = \left[S_1^{(d)}, S_2^{(d)}, \ldots S_e^{(d)} \ldots, S_E^{(d)}\right]$ where $S_e^{(d)}$ is a hidden state variable of a time point. $S_1^{(d)}$ is the initial time, whose hidden state probability depends on $\pi = [\pi_i]$.$S_e^{(d)}$ is an intermediate state hidden state variable, whose hidden state probability depends on $S_{e-1}^{(d)}$ and $A = \left[a_{ij}\right]$ In this work, we exploited a standard HMM with a Gaussian distribution parameterized by μ_k, ε_k as the mean and variance for observation. We mark $S_e^{(d)}\_k$ as a hidden state variable placing hidden state k, $k \in 1, 2, \ldots K$ We can calculate the probability of $X_d^{(r)}$ occurring in the hidden state $S_e^{(d)}\_k$ as shown:

$$p(X_d^{(r)}|S_e^{(d)}\_k) = \frac{1}{(2\pi\varepsilon_k)^{\frac{1}{2}}} e^{-\frac{(X_d^{(r)}-\mu_k)^{\frac{1}{2}}}{2\varepsilon_k}} \quad (1)$$

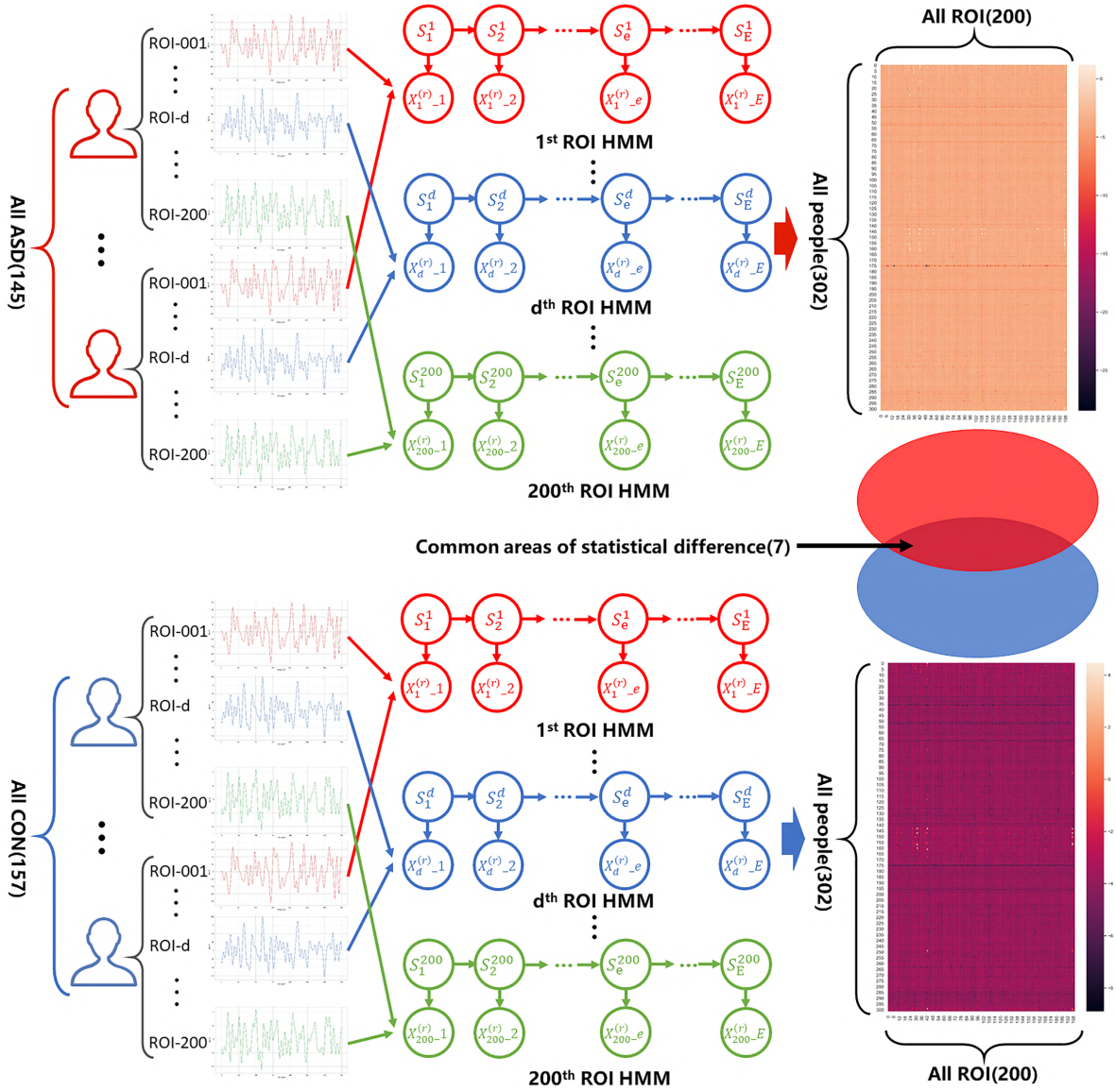

FIGURE 2. Description of training hidden Markov processes and calculation of likelihood values. First, we used the data of all ASDs (145) to train the HMM (ASD MODEL) of each ROI. The likelihood value of all people including ASD and CON was estimated by the trained corresponding ROI model. Then, a rank sum test was performed on the likelihood value of each ROI, and the test value was subjected to FDR correction. Second, we replaced the training model data with all CON (157) (CON MODEL) and repeated the previous steps. Finally, the ROI that showed significant differences in both tests was selected.

Different hidden states obey a Gaussian distribution and have the same calculation form for probability but with unequal mean and variance. Combining $p(X_d^{(r)}|S_e^{(d)}\_k)$ with the transition probability, the probability likelihood of the dth ROI is written as:

$$p\left(X_d^{(r)}\middle|\theta,\emptyset\right) = p(X_d^{(r)}\_1|\pi)\prod_{e=2}^{E} p(S_e^{(d)}|S_{e-1}^{(d)},A) \times \prod_{e=1}^{E} p(X_d^{(r)}\_e|S_e^{(d)}\_k,\emptyset) \quad (2)$$

Maximizing this probability gives the maximum likelihood estimation (MLE) based on the model parameters $\theta = \{\pi, A\}$ and $\emptyset = \mu_k,\ \varepsilon_k{}_{k=1}^{K}$ The detailed construction process of HMM is shown in FIGURE 3. HMM can be solved according to the Expectation-maximization (EM) algorithm, which is a common method for solving maximum likelihood estimate in probability models. Since the likelihood value is too small, we take the natural logarithm of it. Then, in order to eliminate the difference in length of the rs-fMRI BOLD signals, the original likelihood value v is scaled by the length of time series E. Therefore, the final likelihood value L is expressed as follows:

$$L = \frac{1}{E}\ln v \quad (3)$$

D. STATISTICAL ANALYSES

To determine the brain regions with abnormal switching of ASD, we use the rank sum test to statistically analyze the

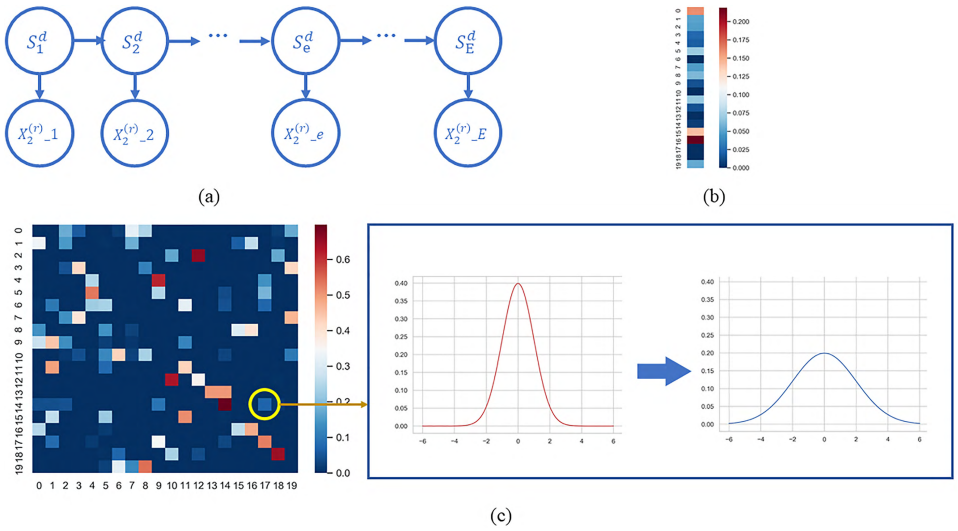

FIGURE 3. HMM parameter visualization (a) HMM process diagram. (b) Schematic diagram of the initial state probability distribution of the HMM. (c) Schematic diagram of a state transition probability matrix. In continuous Gaussian hidden Markov processes, state transitions represent the probability that the distribution to which the observed values obey jumps from one Gaussian process to another.

likelihood values of the two groups of people and correct the statistical P value using false discovery rate correction [34].

III. RESULT

A. STATISTICAL RESULTS OF ROI LIKELIHOOD AND THE CORRELATION WITH CLINICAL SCALE

On the one hand, we used ASD MODEL to calculate the likelihood values of ASD and CON and performed statistical tests. On the other hand, we trained the CON MODEL and repeated the same process. In the end, there were a total of 7 ROIs with significant differences selected using ASD MODEL, all of which were included in ROIs with significant differences selected using CON MODEL. A boxplot of the likelihood values and specific position in the brain for these seven regions is shown in FIGURE 4. In the CC200 brain region, their numbers were 39, 42, 57, 100, 113, 124, and 183. The corresponding AAL partitions are shown in Table 2. We calculated the correlation between ASD and ADOS in 7 ROIs and found that ROI_39 showed a statistically significant negative correlation in the two models (FIGURE 5a, FIGURE 5b). Since most of the clinical scales were only for ASD patients, the IQ scale set was relatively complete, and the IQs of the two groups showed significant differences ($p < 0.01$). IQ was also used as a reference value for clinical diagnosis, so we calculated the correlation between these regions and FIQ. Likelihood values of ROI_113 in both models showed significant positive correlations with FIQ (FIGURE 5c, FIGURE 5d).

B. DIFFERENCE IN LIKELIHOOD VARIANCE

In two models, the variances of the seven ROI likelihood values of ASD and CON were calculated. The two groups of variance values were tested using the paired sample t-test. The p-value of the paired sample T test between the two groups was 0.303 in ASD MODEL and 0.026 in CON MODEL. In CON MODEL, the variance of the likelihood value in the CON group was significantly smaller than that in the ASD group. Although there was no significant difference in another model, we could see that the median variance of the CON group was smaller than that in the ASD group. All in all, the variance of the likelihood value in the CON group was slightly smaller than that in the ASD group.

TABLE 2. Regions showing significant differences in both models.

CC200	AAL	P (ASD MODEL)	P (CON MODEL)
ROI_39	Temporal_Mid_R	0.045	0.01
ROI_39	Temporal_Inf_R	0.045	0.01
ROI_42	Frontal_Mid_Orb_L	0.015	0.004
ROI_42	Frontal_Inf_Orb_L	0.015	0.004
ROI_57	Frontal_Inf_Orb_L	0.038	0.005
ROI_57	Frontal_Mid_Orb_L	0.038	0.005
ROI_100	Temporal_Inf_R	0.025	0.005
ROI_100	Fusiform_R	0.025	0.005
ROI_113	Frontal_Mid_Orb_R	0.015	0.002
ROI_113	Frontal_Mid_R	0.015	0.002
ROI_113	Frontal_Inf_Orb_R	0.015	0.002
ROI_124	Frontal_Mid_Orb_R	0.045	0.005
ROI_124	Frontal_Sup_Orb_R	0.045	0.005
ROI_183	Frontal_Mid_L	0.024	0.004
ROI_183	Frontal_Sup_L	0.024	0.004

C. RESULTS OF CLASSIFICATION

Next, in order to assist in diagnosing ASD objectively with neuroimaging data, we used the seven brain regions extracted by the two models as features. For enriching the features, we also used ASD and CON data to train an HMM (ASD-CON MODEL) corresponding to seven regions jointly.

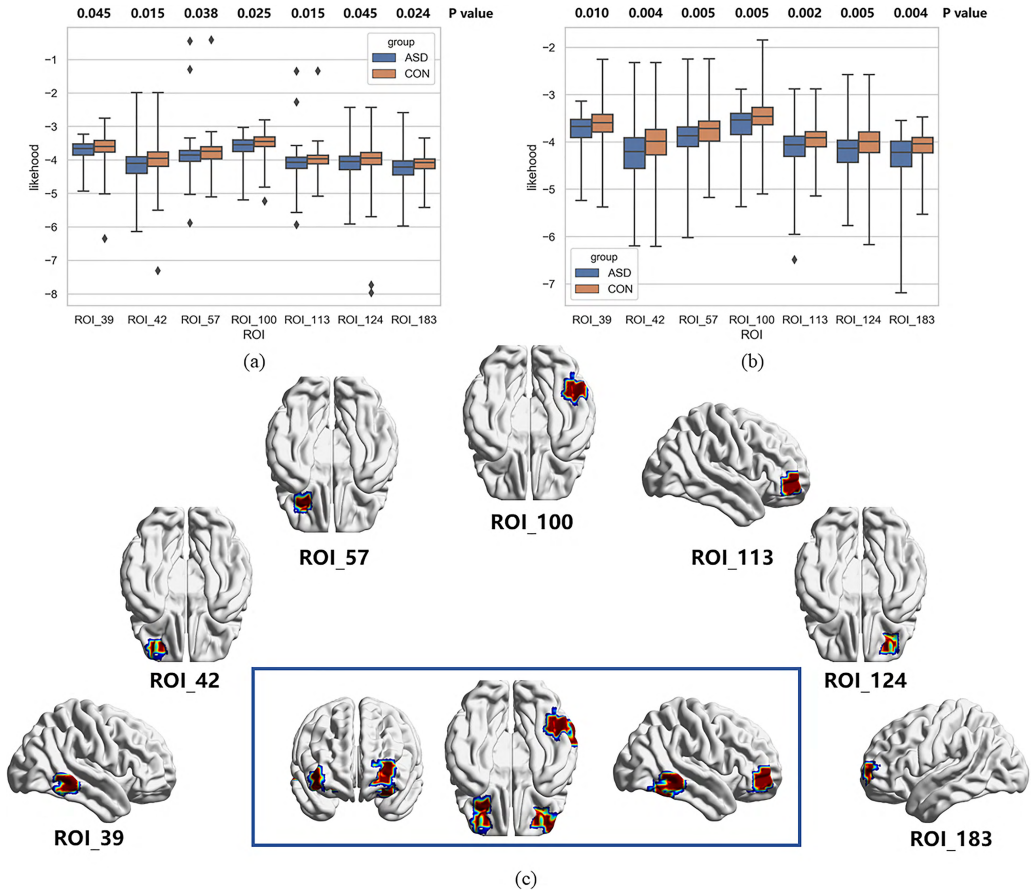

FIGURE 4. **(a) Box chart of the likelihood values of all the data calculated by the ASD MODEL. The top and bottom of each box plot and the upper and lower edges of the middle entity represent the quartile of the entire data. The middle line of the box is the median of the entire data. The points outside the boxplot represent outliers. (b) Box chart that was model trained using only control data. (c) Locations of ROIs with significant differences in the brain. The figure in the blue box comprehensively shows the position of the seven significantly different regions in the brain from three different directions, and the surrounding figures alone show the position of the corresponding subscript ROI.**

It is worth mentioning that the new likelihood values of the seven brain regions had significant differences. Using 302 samples, each consisting of 21 features, we constructed a linear support vector machine classifier. The average classification accuracy rate after ten cross-validations reached 74.9%. The receiver operating characteristic curve (ROC) is shown in FIGURE 6. The average Area Under the Curve (AUC) was 0.8.

IV. DISCUSSION

In this study, we used a two-group cross-localized Hidden Markov Model approach to brain rs-fMRI data. We focused on areas with abnormal dynamics states in ASD and discovered their clinical significance.

A. ABNORMAL BRAIN REGIONS WITH SIGNIFICANT DIFFERENCES

To clearly show where these brain regions belong and to discuss the physiological significance of these brain region abnormalities, we merged these brain regions according to Brodmann divisions. The name and number of the Brodmann areas and corresponding anomaly areas are shown below:

1) Frontopolar area 10: left middle frontal gyrus, right middle frontal gyrus, left superior frontal gyrus;
2) Orbitofrontal area 11,12: left orbital inferior frontal gyrus, right orbital inferior frontal gyrus, left orbital middle frontal gyrus, right orbital middle frontal gyrus, right orbital superior frontal gyrus;
3) Inferior Temporal gyrus 20: right inferior temporal gyrus;
4) Middle Temporal gyrus 21: right middle temporal gyrus;
5) Fusiform gyrus 37: right fusiform gyrus.

Due to the complexity of the causes and symptoms of autism, there were also many abnormal areas. By accounting for the regions listed above, we described their relatedness to ASD in each region, separately.

Neuroimaging studies have implicated the frontopolar regions of the prefrontal cortex in playing a central role in higher cognitive functions such as planning, problem solving, reasoning, and episodic memory retrieval [35]. The significant positive correlation between FIQ and the likelihood value of a part of the ROI in this region could indicate that the function of this region has a greater impact on

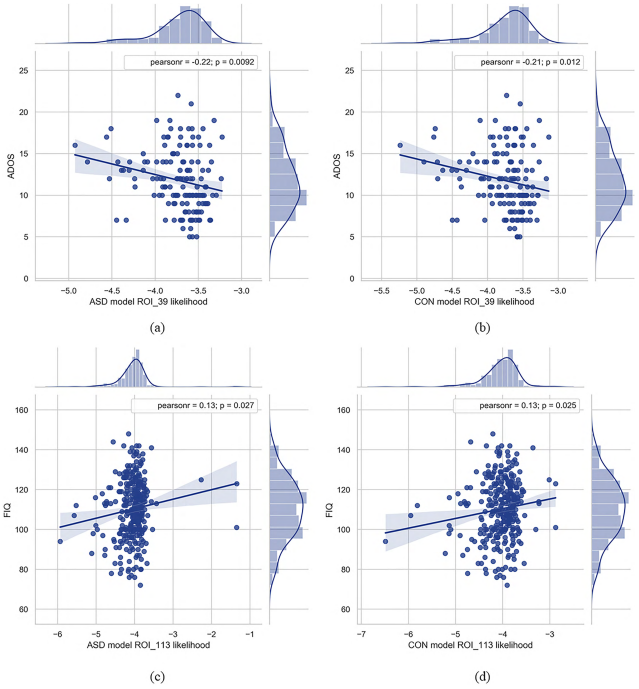

FIGURE 5. Correlation diagram of likelihood value and clinical scale. (a) The correlation ($r = -0.22$, $p = 0.0092$) between ADOS and ASD's ROI_39 likelihood value calculated by ASD MODEL. (b) The correlation ($r = -0.21$, $p = 0.012$) between ADOS and ASD's ROI_39 calculated by CON MODEL data. (c) The correlation ($r = 0.13$, $p = 0.027$) between FIQ and ROI_113, whose likelihood value was calculated by the ASD MODEL. (d) The correlation ($r = 0.13$, $p = 0.025$) between FIQ and ROI_113, whose likelihood value was calculated by the CON MODEL.

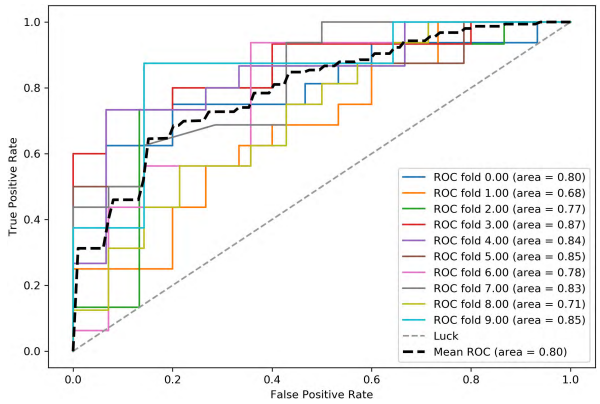

FIGURE 6. ROC curves of ten cross-validations. The values in the parentheses denoted the AUC scores.

IQ. This is not contrary to our general understanding because the functions affected by the frontopolar area are also the abilities examined in the Wechsler Intelligence Scale. Significant abnormalities in this area might explain why ASD showed lower cognitive abilities than CON. Based on neuroanatomy, Eric Courchesne *et al.* [36] also confirmed the abnormality of the prefrontal cortex of ASD. They found that there was overgrowth in this area in ASD, and the number of neurons was significantly higher than that in CON. Combined with the results we obtained, we could infer that the function of the prefrontal cortex might be abnormal because of overgrowth in ASD.

Functions of the orbitofrontal cortex include emotions, decision-making processes and cognition [37]–[39], many of which are abnormal in ASD. In particular, some research [40] pointed out that among the many complications of autism, emotional problems are particularly prominent, and it is often difficult for such individuals to maintain their emotions in a relatively stable state. Our results could show that the emotional problems of autism are caused by abnormalities in the orbitofrontal cortex, which is consistent with the clinical manifestations of autism and previous studies [41], [42]. Obviously, the functions of this region also have an important impact on IQ, so the likelihood of partial ROI correlating with FIQ further confirmed the role of orbitofrontal cortex abnormalities in the pathogenesis of autism.

We will discuss the next three areas together because they are all related to the visual function of the brain. Anatomic, ablation, and physiological evidence all suggest that the neuronal mechanisms that connect vision and memory in primates are located within the inferior temporal cortex, which consists of the middle temporal gyrus and the inferior temporal gyrus anatomically [43]–[45]. The fusiform is involved in both detection and identification of faces [46]. From behavioral experiments and clinical observations, it can be seen that individuals with autism will scan nonfeature areas of the faces significantly more often and core feature areas of faces (such as nose, eyes, etc.) less often [47], [48]. Our findings suggest that disorganized processing of face stimuli is caused by the abnormal activation of the visual area of the brain. Multiple studies involving brain functional connectivity networks and behavioral experiments found that autism is abnormal in the inferior temporal gyrus, middle temporal gyrus, and fusiform gyrus, which supports our results in other ways [49]–[53]. In addition, there is evidence that visuospatial processing is related to the development of core autistic sociocommunicative impairments [54]. In addition to the results mentioned above, the significant negative correlation between the likelihood values of ROIs in this area and the ADOS also proved that the brain status in this area can reflect the severity of autism.

B. STATISTICAL DIFFERENCES OF LIKELIHOOD VARIANCE

According to the results of the statistical test of the different regions and the analysis of FIGURE 4, an interesting phenomenon was found, that is, the likelihood values of the seven different regions of the CON were significantly higher than those of the ASD in the models trained by ASD or CON. According to the statistical test results of the variance in the abnormal area, it could be seen that the variance of the likelihood value in the CON group was significantly smaller than that of the ASD group in CON MODEL. In the other model, although the variance of CON was not statistically significant, we could still see from the trend that its median variance was smaller than that of patients with autism. For this reason, a hypothesis was proposed by us in an attempt

to give a reasonable explanation for the above experimental results: Compared to a resting state of CON, the brain of ASD is often in a chaotic state randomly. When we trained HMMs, a Bayesian probability model, the effects of these random states were averaged. The averaged model was less affected by the random state and was similar to the CON MODEL, so there was not much difference between the two models. However, when we calculated the likelihood value based on such a model, ASD would show a lower likelihood value and a higher variance due to the random state. Rudie et al also found similar results [55]. They found ASD functional connectivity networks had lower clustering (i.e., local efficiency) and shorter average path lengths, which were the characteristics of random connected networks [56].

C. PERFORMANCE IN ASD IDENTIFICATION

After extracting clinically meaningful brain features, a direct way to apply them was to use the extracted features to build a classifier with high accuracy and stability to assist doctors in making more objective clinical diagnosis. Using ASD MODEL, CON MODEL and ASD-CON MODEL calculated the likelihood values of 7 ROIs as features to train the linear support vector machine model. The average accuracy rate reached 74.9%, and the average AUC reached 0.8 after ten cross-validations, which was better than the classification accuracy rate (67%) obtained by Alexandre using functional connectivity networks [57]. The classification results could also explain the effectiveness of our localized ROI and extracted features.

D. LIMITATIONS OF CURRENT RESEARCH

First, in the process of data selection, to ensure the quality of the data we use, complete scales and sex matching can be guaranteed, a large amount of data were eliminated. Although we selected the data from multiple sites without discrimination, the representativeness of the experimental data has not yet been determined. At the same time, because the amount of data is not very large, the final classification results have not been verified on an independent test set. Additionally, we only kept male data because of the inability of men and women to match. Therefore, it is unknown whether the results of this study will be applicable to women with autism. If we can collect enough data for female autism patients in the future, the above results will be supplemented and updated. Furthermore, regarding the selection of the number of hidden states in the experiment, we have combined three factors. The first is research with some good results; the second is to make the average likelihood value obtained by the trained model from the training data as large as possible; the third is the computing power we can currently achieve. We found that within a certain range, the greater the number of hidden states, the larger the mean of the likelihood would be. The larger likelihood values indicated that the currently trained model could better reflect the characteristics of the data. However, when the number of hidden states was large, the mean value of the likelihood increased slowly. Considering our computing power, we finally chose 20 hidden states. Exploring the physiological meaning of the hidden state and the results in the higher hidden state is our next work plan.

V. CONCLUSION

In conclusion, the present study demonstrated that the abnormal areas in the frontopolar area, orbitofrontal area, inferior temporal gyrus, middle temporal gyrus, and fusiform gyrus are prominent features of ASD and closely related to the decline in clinical function. This 'two-group cross-localized Hidden Markov Model' provides a robust and powerful framework for understanding the dysfunctional brain architecture in ASD and auxiliary diagnosis.

REFERENCES

[1] B. C. Riedel, N. Jahanshad, and P. M. Thompson, "Graph theoretical approaches towards understanding differences in frontoparietal and default mode networks in autism," in *Proc. IEEE 14th Int. Symp. Biomed. Imag. (ISBI)*, Apr. 2017, pp. 460–463.

[2] E. T. Bullmore, S. Frangou, and R. M. Murray, "The dysplastic net hypothesis: An integration of developmental and dysconnectivity theories of schizophrenia," *Schizophrenia Res.*, vol. 28, nos. 2–3, pp. 143–156, Dec. 1997.

[3] B. S. Khundrakpam, J. D. Lewis, P. Kostopoulos, F. Carbonell, and A. C. Evans, "Cortical thickness abnormalities in autism spectrum disorders through late childhood, adolescence, and adulthood: A large-scale MRI study," *Cerebral Cortex*, vol. 27, no. 3, pp. 1721–1731, Mar. 2017.

[4] M. Casanova and J. Trippe, "Radial cytoarchitecture and patterns of cortical connectivity in autism," *Phil. Trans. Roy. Soc. B, Biol. Sci.*, vol. 364, no. 1522, pp. 1433–1436, May 2009.

[5] P. Barttfeld, B. Wicker, S. Cukier, S. Navarta, S. Lew, and M. Sigman, "A big-world network in ASD: Dynamical connectivity analysis reflects a deficit in long-range connections and an excess of short-range connections," *Neuropsychologia*, vol. 49, no. 2, pp. 254–263, Jan. 2011.

[6] R. Chen, Y. Jiao, and E. H. Herskovits, "Structural MRI in autism spectrum disorder," *Pediatric Res.*, vol. 69, no. 5 Part 2, pp. 63–68, May 2011.

[7] A. Di Martino, "The autism brain imaging data exchange: Towards a large-scale evaluation of the intrinsic brain architecture in autism," *Mol. Psychiatry*, vol. 19, no. 6, pp. 659–667, 2014.

[8] E. Jun, E. Kang, J. Choi, and H.-I. Suk, "Modeling regional dynamics in low-frequency fluctuation and its application to autism spectrum disorder diagnosis," *NeuroImage*, vol. 184, pp. 669–686, Jan. 2019.

[9] J. V. Hull, L. B. Dokovna, Z. J. Jacokes, C. M. Torgerson, A. Irimia, and J. D. Van Horn, "Resting-state functional connectivity in autism spectrum disorders: A review," *Frontiers Psychiatry*, vol. 7, p. 205, Jan. 2017.

[10] M. D. Fox, A. Z. Snyder, J. L. Vincent, M. Corbetta, D. C. Essen, and M. E. Raichle, "The human brain is intrinsically organized into dynamic, anticorrelated functional networks," *Proc. Nat. Acad. Sci. USA*, vol. 102, no. 27, pp. 9673–9678, 2005.

[11] C. Sorg, V. Riedl, M. Muhlau, V. D. Calhoun, T. Eichele, L. Laer, A. Drzezga, H. Forstl, A. Kurz, C. Zimmer, and A. M. Wohlschlager, "Selective changes of resting-state networks in individuals at risk for Alzheimer's disease," *Proc. Nat. Acad. Sci. USA*, vol. 104, no. 47, pp. 18760–18765, Nov. 2007.

[12] J. S. Anderson, J. A. Nielsen, A. L. Froehlich, M. B. DuBray, T. J. Druzgal, A. N. Cariello, J. R. Cooperrider, B. A. Zielinski, C. Ravichandran, P. T. Fletcher, A. L. Alexander, E. D. Bigler, N. Lange, and J. E. Lainhart, "Functional connectivity magnetic resonance imaging classification of autism," *Brain*, vol. 134, no. 12, pp. 3742–3754, Dec. 2011.

[13] E. P. K. Pua, C. B. Malpas, S. C. Bowden, and M. L. Seal, "Different brain networks underlying intelligence in autism spectrum disorders," *Hum. Brain Mapping*, vol. 39, no. 8, pp. 3253–3262, Aug. 2018.

[14] B. Rashid, L. M. E. Blanken, R. L. Muetzel, R. Miller, E. Damaraju, M. R. Arbabshirani, E. B. Erhardt, F. C. Verhulst, A. van der Lugt, V. W. V. Jaddoe, H. Tiemeier, T. White, and V. Calhoun, "Connectivity dynamics in typical development and its relationship to autistic traits and autism spectrum disorder," *Hum. Brain Mapping*, vol. 39, no. 8, pp. 3127–3142, Aug. 2018.

[15] E. A. H. von dem Hagen, R. S. Stoyanova, S. Baron-Cohen, and A. J. Calder, "Reduced functional connectivity within and between—Social' resting state networks in autism spectrum conditions," *Social Cognit. Affect. Neurosci.*, vol. 8, no. 6, pp. 694–701, Aug. 2013.
[16] A. R. McIntosh, F. L. Bookstein, J. V. Haxby, and C. L. Grady, "Spatial pattern analysis of functional brain images using partial least squares," *NeuroImage*, vol. 3, no. 3, pp. 143–157, Jun. 1996.
[17] R. Salvador, J. Suckling, M. R. Coleman, J. D. Pickard, D. Menon, and E. Bullmore, "Neurophysiological architecture of functional magnetic resonance images of human brain," *Cerebral Cortex*, vol. 15, no. 9, pp. 1332–1342, Sep. 2005.
[18] H. Lee, D. Soo Lee, H. Kang, B.-N. Kim, and M. K. Chung, "Sparse brain network recovery under compressed sensing," *IEEE Trans. Med. Imag.*, vol. 30, no. 5, pp. 1154–1165, May 2011.
[19] W. Sun and L. Li, "STORE: Sparse tensor response regression and neuroimaging analysis," *J. Mach. Learn. Res.*, vol. 18, pp. 135:1–135:37, 2017.
[20] M. Assaf, K. Jagannathan, V. D. Calhoun, L. Miller, M. C. Stevens, R. Sahl, J. G. O'Boyle, R. T. Schultz, and G. D. Pearlson, "Abnormal functional connectivity of default mode sub-networks in autism spectrum disorder patients," *NeuroImage*, vol. 53, no. 1, pp. 247–256, Oct. 2010.
[21] S. J. Broyd, C. Demanuele, S. Debener, S. K. Helps, C. J. James, and E. J. S. Sonuga-Barke, "Default-mode brain dysfunction in mental disorders: A systematic review," *Neurosci. Biobehavioral Rev.*, vol. 33, no. 3, pp. 279–296, Mar. 2009.
[22] A. L. Alexander, J. E. Lee, M. Lazar, R. Boudos, M. B. DuBray, T. R. Oakes, J. N. Miller, J. Lu, E.-K. Jeong, and W. M. McMahon, "Diffusion tensor imaging of the corpus callosum in autism," *NeuroImage*, vol. 34, no. 1, pp. 61–73, 2007.
[23] D. P. Kennedy, E. Redcay, and E. Courchesne, "Failing to deactivate: Resting functional abnormalities in autism," *Proc. Nat. Acad. Sci. USA*, vol. 103, no. 21, pp. 8275–8280, May 2006.
[24] M. D. Fox and M. E. Raichle, "Spontaneous fluctuations in brain activity observed with functional magnetic resonance imaging," *Nature Rev. Neurosci.*, vol. 8, no. 9, pp. 700–711, Sep. 2007.
[25] T. Nakai, E. Bagarinao, K. Matsuo, Y. Ohgami, and C. Kato, "Dynamic monitoring of brain activation under visual stimulation using fMRI the advantage of real-time fMRI with sliding window glm analysis," *J. Neurosci. methods*, vol. 157, no. 1, pp. 158–167, 2006.
[26] H.-I. Suk, C.-Y. Wee, S.-W. Lee, and D. Shen, "State-space model with deep learning for functional dynamics estimation in resting-state fMRI," *NeuroImage*, vol. 129, pp. 292–307, Apr. 2016.
[27] D. Vidaurre, R. Abeysuriya, R. Becker, A. J. Quinn, F. Alfaro-Almagro, S. M. Smith, and M. W. Woolrich, "Discovering dynamic brain networks from big data in rest and task," *NeuroImage*, vol. 180, pp. 646–656, Oct. 2018.
[28] R. Hindriks, M. H Adhikari, Y. Murayama, M. Ganzetti, D. Mantini, N. K. Logothetis, and G. Deco, "Can sliding-window correlations reveal dynamic functional connectivity in resting-state fMRI?" *NeuroImage*, vol. 127, pp. 242–256, Oct. 2016.
[29] Y. Wang, S. M. Resnick, and C. Davatzikos, "Analysis of spatio-temporal brain imaging patterns by hidden Markov models and serial MRI images," *Hum. Brain Mapping*, vol. 35, no. 9, pp. 4777–4794, Sep. 2014.
[30] H. Eavani, T. D. Satterthwaite, R. E. Gur, R. C. Gur, and A. Davatzikos, "Unsupervised learning of functional network dynamics in resting state fMRI," in *Proc. Int. Conf. Inf. Process. Med. Imag.* Berlin, Germany: Springer, 2013, pp. 426–437.
[31] R. Duan, H. Man, W. Jiang, and W.-C. Liu, "Activation detection on fMRI time series using hidden Markov model," in *Proc. 2nd Int. IEEE EMBS Conf. Neural Eng.*, Dec. 2005, pp. 510–513.
[32] O. Nikdelfaz and S. Jalili, "Disease genes prediction by HMM based PU-learning using gene expression profiles," *J. Biomed. Informat.*, vol. 81, pp. 102–111, May 2018.
[33] C. Craddock, Y. Benhajali, C. Chu, F. Chouinard, A. Evans, A. Jakab, B. S. Khundrakpam, J. D. Lewis, Q. Li, and M. Milham, "The neuro bureau preprocessing initiative: Open sharing of preprocessed neuroimaging data and derivatives," *Neuroinformatics*, vol. 41, 2013.
[34] Y. Benjamini and Y. Hochberg, "Controlling the false discovery rate: A practical and powerful approach to multiple testing," *J. Roy. Stat. Soc., B Methodol.*, vol. 57, no. 1, pp. 289–300, Jan. 1995.
[35] T. S. Braver and S. R. Bongiolatti, "The role of frontopolar cortex in subgoal processing during working memory," *NeuroImage*, vol. 15, no. 3, pp. 523–536, Mar. 2002.
[36] J. A. Stockman, "Neuron number and size in prefrontal cortex of children with autism," *Yearbook Pediatrics*, vol. 2013, pp. 395–397, Jan. 2013.
[37] A. Y. Hardan, R. R. Girgis, A. L. T. Lacerda, O. Yorbik, M. Kilpatrick, M. S. Keshavan, and N. J. Minshew, "Magnetic resonance imaging study of the orbitofrontal cortex in autism," *J. Child Neurol.*, vol. 21, no. 10, pp. 866–871, Oct. 2006.
[38] J. T. Morgan, G. Chana, I. Abramson, K. Semendeferi, E. Courchesne, and I. P. Everall, "Abnormal microglial–neuronal spatial organization in the dorsolateral prefrontal cortex in autism," *Brain Res.*, vol. 1456, pp. 72–81, May 2012.
[39] H. Watanabe, M. Nakamura, T. Ohno, T. Itahashi, E. Tanaka, H. Ohta, T. Yamada, C. Kanai, A. Iwanami, N. Kato, and R. Hashimoto, "Altered orbitofrontal sulcogyral patterns in adult males with high-functioning autism spectrum disorders," *Social Cognit. Affect. Neurosci.*, vol. 9, no. 4, pp. 520–528, Apr. 2014.
[40] C. Gillberg And and E. Billstedt, "Autism and asperger syndrome: Coexistence with other clinical disorders," *Acta Psychiatrica Scandinavica*, vol. 102, no. 5, pp. 321–330, Nov. 2000.
[41] S. Baron-Cohen, H. A. Ring, S. Wheelwright, E. T. Bullmore, M. J. Brammer, A. Simmons, and S. C. R. Williams, "Social intelligence in the normal and autistic brain: An fMRI study," *Eur. J. Neurosci.*, vol. 11, no. 6, pp. 1891–1898, Jun. 1999.
[42] M. A. Sabbagh, "Understanding orbitofrontal contributions to theory-of-mind reasoning: Implications for autism," *Brain Cognition*, vol. 55, no. 1, pp. 209–219, Jun. 2004.
[43] M. J. Buckley, D. Gaffan, and E. A. Murray, "Functional double dissociation between two inferior temporal cortical areas: Perirhinal cortex versus middle temporal gyrus," *J. Neurophysiol.*, vol. 77, no. 2, pp. 587–598, Feb. 1997.
[44] J. J. DiCarlo, D. Zoccolan, and N. C. Rust, "How does the brain solve visual object recognition?" *Neuron*, vol. 73, no. 3, pp. 415–434, 2012.
[45] C. G. Gross, "How inferior temporal cortex became a visual area," *Cerebral Cortex*, vol. 4, no. 5, pp. 455–469, 1994.
[46] K. Grill-Spector, N. Knouf, and N. Kanwisher, "The fusiform face area subserves face perception, not generic within-category identification," *Nature Neurosci.*, vol. 7, no. 5, pp. 555–562, May 2004.
[47] S. Naumann, U. Senftleben, M. Santhosh, J. McPartland, and S. J. Webb, "Neurophysiological correlates of holistic face processing in adolescents with and without autism spectrum disorder," *J. Neurodevelopmental Disorders*, vol. 10, no. 1, p. 27, Dec. 2018.
[48] J. W. Tanaka and A. Sung, "The 'eye avoidance' hypothesis of autism face processing," *J. Autism Develop. Disorders*, vol. 46, no. 5, pp. 1538–1552, 2016.
[49] J. Cai, X. Hu, K. Guo, P. Yang, M. Situ, and Y. Huang, "Increased left inferior temporal gyrus was found in both low function autism and high function autism," *Frontiers Psychiatry*, vol. 9, p. 542, Oct. 2018.
[50] M. S. Gaffrey, N. M. Kleinhans, F. Haist, N. Akshoomoff, A. Campbell, E. Courchesne, and R.-A. Müller, "A typical participation of visual cortex during word processing in autism: An fMRI study of semantic decision," *Neuropsychologia*, vol. 45, no. 8, pp. 1672–1684, 2007.
[51] H. Koshino, R. K. Kana, T. A. Keller, V. L. Cherkassky, N. J. Minshew, and M. A. Just, "FMRI investigation of working memory for faces in autism: Visual coding and underconnectivity with frontal areas," *Cerebral Cortex*, vol. 18, no. 2, pp. 289–300, Feb. 2008.
[52] W. Sato, M. Toichi, S. Uono, and T. Kochiyama, "Impaired social brain network for processing dynamic facial expressions in autism spectrum disorders," *BMC Neurosci.*, vol. 13, no. 1, p. 99, Dec. 2012.
[53] J. Xu, C. Wang, Z. Xu, T. Li, F. Chen, K. Chen, J. Gao, J. Wang, and Q. Hu, "Specific functional connectivity patterns of middle temporal gyrus subregions in children and adults with autism spectrum disorder," *Autism Res.*, vol. 13, no. 3, pp. 410–422, Mar. 2020.
[54] B. Keehn, P. Shih, L. A. Brenner, J. Townsend, and R.-A. Müller, "Functional connectivity for an Island of sparing in autism spectrum disorder: An fMRI study of visual search," *Hum. Brain Mapping*, vol. 34, no. 10, pp. 2524–2537, Oct. 2013.
[55] J. D. Rudie, J. A. Brown, D. Beck-Pancer, L. M. Hernandez, E. L. Dennis, P. M. Thompson, S. Y. Bookheimer, and M. Dapretto, "Altered functional and structural brain network organization in autism," *NeuroImage*, vol. 2, pp. 79–94, Dec. 2013.
[56] O. Sporns, "The non-random brain: Efficiency, economy, and complex dynamics," *Frontiers Comput. Neurosci.*, vol. 5, p. 5, Aug. 2011.
[57] A. Abraham, M. P. Milham, A. Di Martino, R. C. Craddock, D. Samaras, B. Thirion, and G. Varoquaux, "Deriving reproducible biomarkers from multi-site resting-state data: An autism-based example," *NeuroImage*, vol. 147, pp. 736–745, Feb. 2017.